Hindawi
Geofluids
Volume 2022, Article ID 2124853, 11 pages
https://doi.org/10.1155/2022/2124853

Research Article

Study on the Destructive Effect of Small Faults on Coal Pore Structure

Jianbao Liu,[1,2] **Zhimin Song**,[1,2,3] **Bing Li**,[1] **Jiangang Ren**,[1] **Feng Chen**,[1] **Ming Xiao**,[1] **and Chengtao Yang**[4]

[1]*Henan University of Engineering, Zhengzhou 451191, China*
[2]*Henan Polytechnic University, Jiaozuo 454000, China*
[3]*North China University of Water Resources and Electric Power, Zhengzhou 450046, China*
[4]*Henan Energy and Chemical Industry Group Research Institute Co., Ltd, Zhengzhou 450046, China*

Correspondence should be addressed to Zhimin Song; songzhimin1961@hotmail.com and Chengtao Yang; byctat@163.com

Received 28 July 2022; Revised 16 August 2022; Accepted 1 September 2022; Published 3 October 2022

Academic Editor: Jianchao Cai

Small fault area in coal mine has great risk of coal and gas outburst. However, the damage effect of small faults on coal pore structure still lacks systematic research. Taking a small reverse fault under Pingmei No. 2 mine as an example, this paper collects the hanging wall coal samples within 5 m from the fault plane and the coal samples 50 m from the fault plane, where there is no fault development. The pore structure characteristics of the two coal samples were analyzed and compared by means of a scanning electron microscope, mercury injection, liquid nitrogen adsorption, and Raman spectroscopy. The test results show that compared with the coal samples without faults, the coal samples at faults form micron-scale fracture zones with constant spacing, stable occurrence, and flat two walls. The pore volume and pore specific surface area of different pore sizes increase, the pore peak of mesopore (100~1000 nm) shifts from 1000 nm to 200~400 nm, and its connectivity is enhanced. The number of micropores (<10 nm) increased significantly, and the ink bottle type pores developed. Faulting also has a certain impact on the macromolecular structure of coal, which shows that the D peak area decreases and the area of G peak increases, indicating that the order degree of macromolecular structure of coal increases.

1. Introduction

Coal resources are the main energy for economic development of China presently and also in the near future [1]. It is predicted that China will consume about 50% of its resources from coal by 2050. Under the guidance of the dual-carbon strategy, the intelligentization and low carbon emission of coal production are an inevitable trend of development [2–4]. On the road of intelligent development of coal mines, coal and gas outburst is still the biggest obstacle to safe production. Coal and gas outbursts are closely related to the development of structural belts. Production practice has proved that where there are outbursts, there are many structures nearby, especially small faults. Small faults often form stress concentration, destroy the coal body, form fractures in the coal, reform the pore structure of the coal, provide a place for gas enrichment, and form a gas anomaly area around the fault [5–8]. When the mining activity is close to the fault, the stress balance in the gas anomaly area is broken, and the high-pressure gas is released instantaneously, resulting in coal and gas outburst.

Previous studies on the development of fractures and pores of coal and rock near small faults are mainly realized by similarity simulation, numerical simulation, and sampling analysis [9–12]. Based on different research methods, the achieved results can be divided into macro- and microaspects. In the macroscopic aspect, the quantitative prediction of fractures in the process of fault development is mainly realized by means of physical simulation and numerical simulation. It is found that the fractures near the fault are significantly increased, the plastic failure area is distributed within a certain range from the fault,

and the strength of coal and rock in the area is significantly lower than that in other areas. The farther away from the fault plane, the smaller the area of the plastic zone, and the damage degree of the hanging wall of the fault is greater than that of the footwall [13–17]. In the microscopic aspect, by means of scanning electron microscopy, mercury porosimetry, liquid nitrogen adsorption, and other detection methods, it is mainly found that macropores and fractures are developed in coal samples near the fault plane. Their specific surface area and pore volume are improved to a certain extent, and the pores and fractures have better connectivity [18–22].

The above research results show that the number of fractures near small faults increases and the pore structure of coal is improved, which provides storage space for free gas. However, the research on the effect of small faults on the pore structure of coal is still lacking systematically. In this paper, taking a small reverse fault in Pingmei No. 2 mine as an example, coal samples at different distances from the small fault were collected and analyzed by scanning electron microscopy, mercury intrusion, liquid nitrogen, and Raman spectroscopy to study the damage of the small fault to the pore structure of coal. The research results have theoretical significance for the theoretical study of coal and gas outburst in the small fault zone and have practical value for preventing and controlling gas disasters in coal mines.

2. Samples and Methodology

2.1. Samples. The coal samples were collected from the working face of No. 1_5 coal seam in a mine in Pingmei No. 2 mine. The 1_5 coal seam is the lower part of the Taiyuan Formation, 46.52~67.17 m above the 2_1 coal seam. The 1_5 coal seam is well developed in whole mine field, and its thickness is 0.26~3.9 m; the average is 1.52 m. The coal seam recoverability index is 0.83, and the coal thickness variation coefficient is 48.07%, which show that the coal seam is relatively stable and most mineable. The coal seam structure is more complex, generally containing 1 to 3 layers of gangue. The roof of the coal seam is limestone L_5, and the bottom plate is mudstone or limestone L_4. The floor elevation is -17 m~-800 m, and the buried depth is 137~1145 m. The gas content of the coal seam is generally low, and the highest value is 5.25 cm ^{3}/g.

A reverse fault with a drop of 0.8~2.7 m, an inclination of 95°, and an inclination of 10° is exposed in the wind tunnel of the working face. The total length of the roadway is 1880 m. The fault is located in the middle of the roadway, 500 m away from the cut hole in the west. The data of gas content shows that the closer the distance to the fault plane, the greater the gas content is. Two coal samples were collected. The coal sample collected within 5 m of the fault plane was marked as A1. The coal sample collected 50 m away from the fault plane was marked as A2 (Figure 1). Figure 1 shows that A1 coal sample is composed of many small fragments, while A2 coal sample is a single block of coal. The coal quality test results are shown as follows (Table 1), and the coal is 1/3 coking coal.

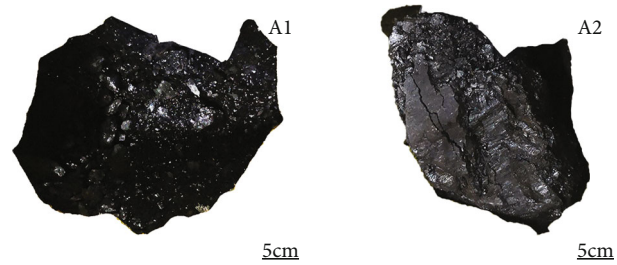

Figure 1: Coal samples collected at different locations.

Table 1: Proximate analysis of coal samples.

Sample	Analysis project			
	M_{ad} (%)	A_{ad} (%)	V_{ad} (%)	$Q_{gr,ad}$ (MJ·kg^{-1})
A1	0.56	14.83	28.86	29.69
A2	0.65	28.88	31.80	24.39

Note: M_{ad} (%) is moisture of air dry basis; A_{ad} (%) is ash of air dry basis; V_{ad} (%) is volatile matter of air dry basis; $Q_{gr,ad}$ (MJ·kg^{-1}) is the high calorific value of air dry basis.

2.2. Methodology. In this paper, the development of macrofractures in coal samples is detected by a scanning electron microscope (SEM). SEM is mainly used to observe the surface information of materials. It can be magnified hundreds of thousands of times to observe nanoscale objects [23–25]. In this experiment, a Quanta 250 scanning electron microscope from Czech FEI Company was used. The maximum pressure of the sample chamber was 2600 Pa, the acceleration voltage was 200 V~30 KV, and the resolution was up to 3 nm. The collected coal samples are cut into blocks and subjected to grinding, polishing, purging, drying, and conductive treatment.

Mercury porosimetry and liquid nitrogen adsorption were used to observe the pore structure of coal samples. Mercury porosimetry adopts the American Micromeritics AutoPore IV 9510, the maximum pressure can reach 228 MPa, and the analytical pore size range is 5 nm~800 μm. The sample particle size of 1~5 mm was adopted for this test, and the samples were dried at 105°C to constant weight before the test.

Liquid nitrogen adsorption is an important method to study the micropore characteristics of porous media. Combined with porosimetry, it forms a pore characterization system from meso to micro [26]. Liquid nitrogen adsorption is an important method to study the pore structure of porous media. The specific surface area, pore volume, pore size distribution, adsorption-desorption curve, and other parameters of porous media are obtained by using the adsorption performance of porous media to gas molecules [27–29]. Micromeritics ASAP2460 was adopted to carry out liquid nitrogen adsorption in this study. The range of pore sizes that can be tested includes pore diameter $\varphi < 2$ nm. The particle sample below 3 mm is used this time, and the sample mass is more than 100 mg. Before the liquid nitrogen adsorption test, the coal sample needs to be heated at

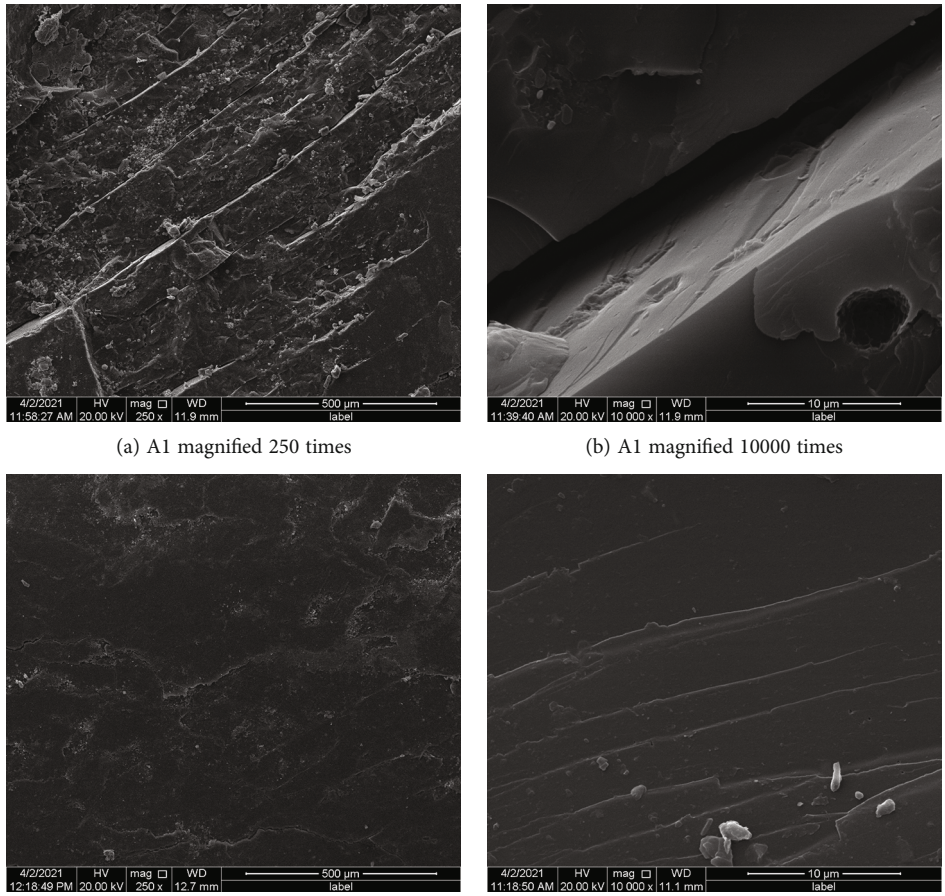

(a) A1 magnified 250 times (b) A1 magnified 10000 times

(c) A2 magnified 250 times (d) A2 magnified 10000 times

Figure 2: SEM images of coal samples at different positions. (a, b) Show fracture groups with straight walls, stable strikes, and close spacing. (c, d) Show wavy beddings.

110°C for 8 hours to discharge the impurities in the coal sample through heating and evaporation.

In order to study whether the small fault has an impact on the macromolecular structure of coal, we carried out Raman spectrum analysis. Raman spectroscopy is a nondestructive and rapid detection technique, which can be used to reveal the disorder of the amorphous structure and the order of the crystallite structure inside the coal sample. The Raman effect originates from the vibration and rotation of molecules and lattices, so we can obtain the relevant parameters such as molecular vibration level, lattice vibration level, and rotation level from the Raman spectrum [30–32]. A Horiba Evolution Raman spectrometer is adopted in this study, and a laser with a wavelength of 532 nm is selected for testing. The size of coal samples requires a minimum of $2 * 2$ mm and a maximum of $5 * 5$ cm.

3. Results and Discussions

3.1. Scanning Electron Microscope. The SEM results of coal samples show that coal sample A1 which is near the fault layer develops fracture groups with straight walls, stable strikes, and close spacing, while coal sample A2 which is far from the fault has no such phenomenon and only develops wavy beddings (Figure 2). It shows that in the process of small fault formation, which is mainly under the action of shear stress, the coal body structure near the fault plane is damaged, and the directional arrangement of shear joint groups is formed.

3.2. Mercury Porosimetry

3.2.1. Mercury Injection-Ejection Curve. Figure 3 shows the mercury injection-ejection curves of coal samples at different distances from the small fault. The figure shows that the total amount of mercury injected into the coal sample A1 at the fault is greater than that of the coal sample A2 without the fault, and the retained mercury at the end of the mercury ejection curve is smaller than that of the coal sample A2. This indicates that the pore connectivity of coal sample A1 at the fault has been improved.

3.2.2. Comparison of Pore Volume. The pore volume of coal sample can be calculated from the volume differential of mercury intrusion [33]. It can be seen from Figure 4 that compared with the coal sample A2, the peak pore volume of the coal sample A1 is shifted to a smaller size. This may be related to the enhanced connectivity between pores

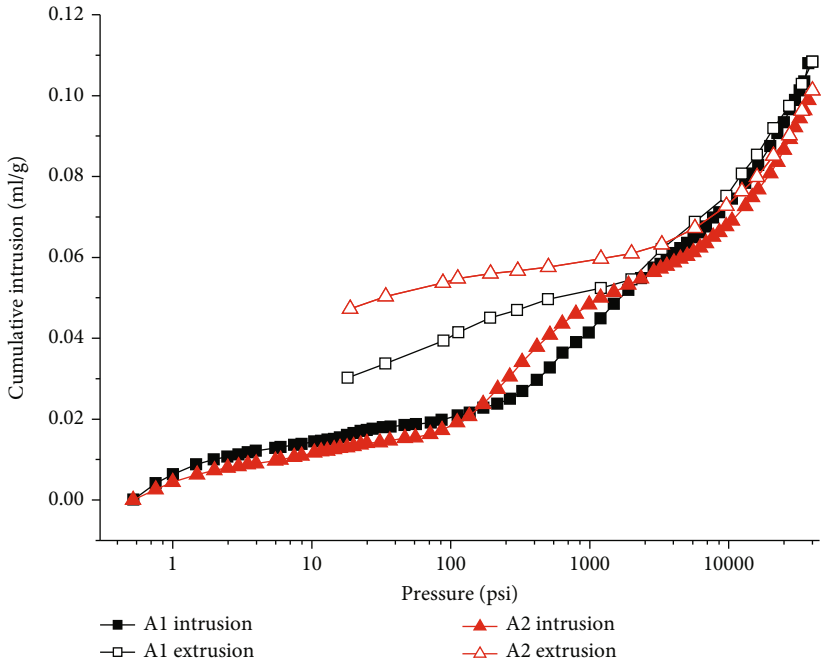

Figure 3: Mercury injection-ejection curve of coal samples at different positions.

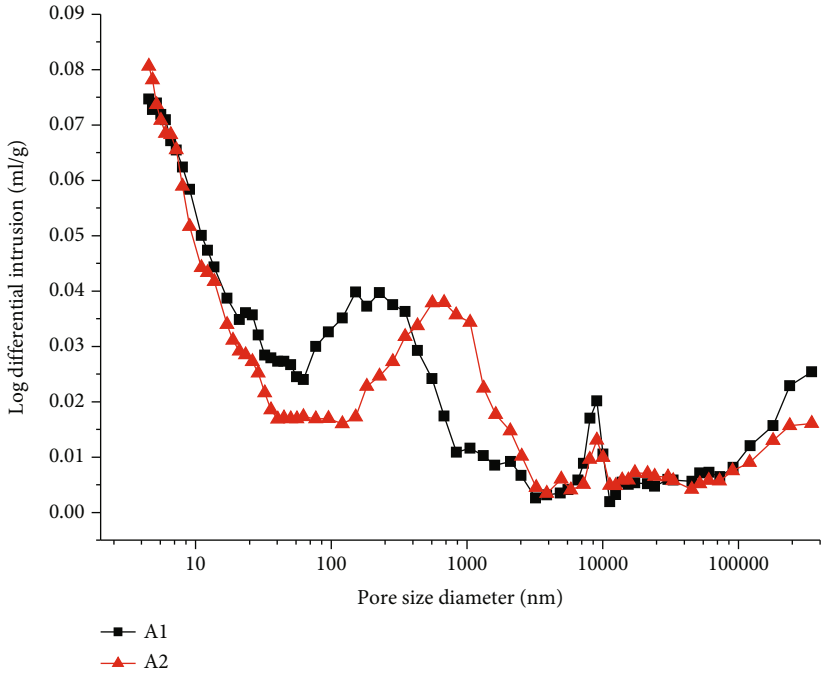

Figure 4: Comparison of mercury injection pore volume of coal samples at different positions.

under the action of faults. The development of fractures cuts and destroys the original larger pore size, causing the pore size peak to shift from 1000 nm to 200~400 nm. It shows that the fault has a significant effect on the mesopores (100 nm~1 μm) of coal.

3.2.3. Comparison of Specific Surface Area. The specific surface area and pore volume complement each other, reflecting the distribution characteristics of the pore structure of the coal from different sides. It can be seen from the cumulative specific surface area distribution diagram

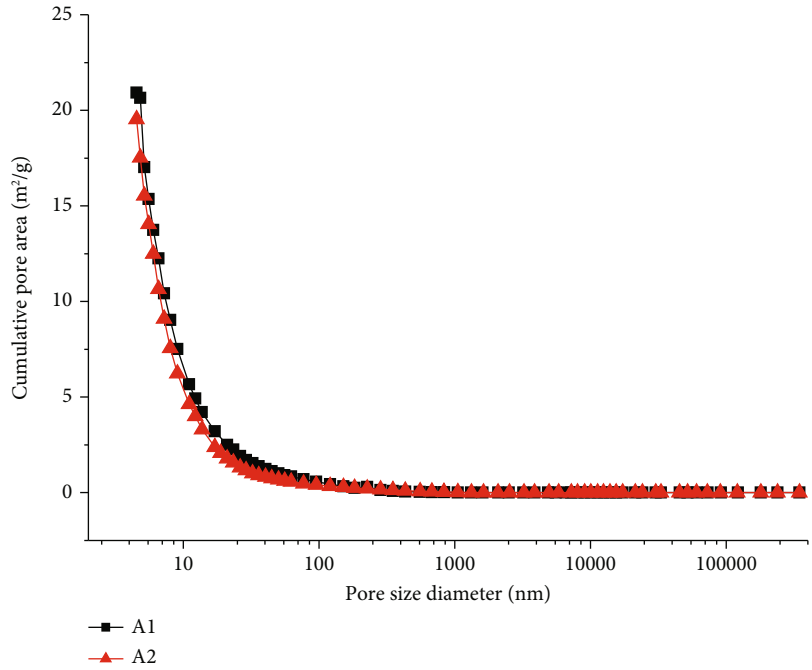

Figure 5: Comparison of mercury injection specific surface area of coal samples at different positions.

that the cumulative specific surface area of coal samples at different positions increases exponentially with the decrease of pore size. The cumulative specific surface area of the coal sample A1 at the fault is slightly larger than that of the coal sample A2 without the fault (Figure 5). The test results show that the fault also has a certain influence on the micropores (<10 nm) and transition pores (10~ 100 nm).

Pore specific surface area, porosity, median pore diameter, bending coefficient, and fractal dimension of coal samples at different positions are shown in Table 2. It can be seen that the porosity, total specific surface area, total pore volume, and median pore diameter of coal sample A1 at the fault have increased, and the specific surface area of the mesopores has increased by about 30%. It also shows from the side view that the small faults have the transformation effect on the macropores and the mesopores, especially the influence on the mesopores which is obvious. The test results also showed that the bending coefficient and fractal dimension of the pores decreased, indicating that the pore morphology became simpler and the connectivity was enhanced.

Table 2: Comparison of mercury porosimetry parameters of coal samples.

Sample	A1	A2
Total pore volume (cm^3/g)	1.1×10^{-1}	1.0×10^{-1}
Micropore volume (cm^3/g)	2.1×10^{-2}	2.0×10^{-2}
Transition pore volume (cm^3/g)	3.6×10^{-2}	2.8×10^{-2}
Mesopore pore volume (cm^3/g)	3.1×10^{-2}	2.6×10^{-2}
Macropore pore volume (cm^3/g)	2.4×10^{-2}	2.8×10^{-2}
Total specific surface area (m^2/g)	2.1×10^{1}	1.9×10^{1}
Micropore specific surface area (m^2/g)	1.34×10^{1}	1.33×10^{1}
Transition pore specific surface area (m^2/g)	6.9	5.8
Mesopore specific surface area (m^2/g)	5.5×10^{-1}	3.7×10^{-1}
Macropore specific surface area (m^2/g)	1.8×10^{-3}	4.0×10^{-2}
Porosity (%)	14.4%	12.7%
Median pore size (nm)	7.2	6.9
Bending factor	2.072	2.076
Fractal dimension	2.811	2.850

3.3. Liquid Nitrogen Adsorption Test

3.3.1. Isotherm Adsorption-Desorption Curves. The isotherms of coal samples at different locations all belong to category IV isotherms (Figure 6). The adsorption-desorption isotherms of liquid nitrogen show that the maximum adsorption capacity of coal sample A2 without faults is only 1.4 cm^3/g, while the maximum adsorption capacity of coal sample A1 at faults reaches more than 2.6 cm^3/g, an increase of nearly 1 times. Therefore, the pore structure of the coal body is reformed due to faulting, and the number of pores is greatly increased. In addition, the A1 hysteresis loop of the coal sample at the fault is more obvious, and there is an inflection point on the liquid nitrogen adsorption regression curve in the region of the relative pressure of 0.4~0.5, indicating that there are abundant ink bottle holes in the coal sample.

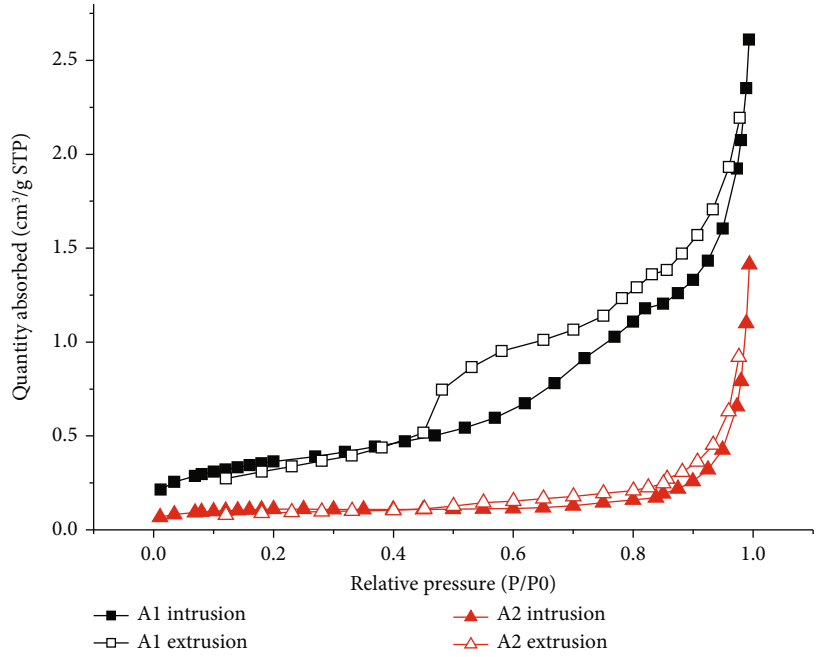

Figure 6: Liquid nitrogen adsorption-desorption curves of coal samples at different positions.

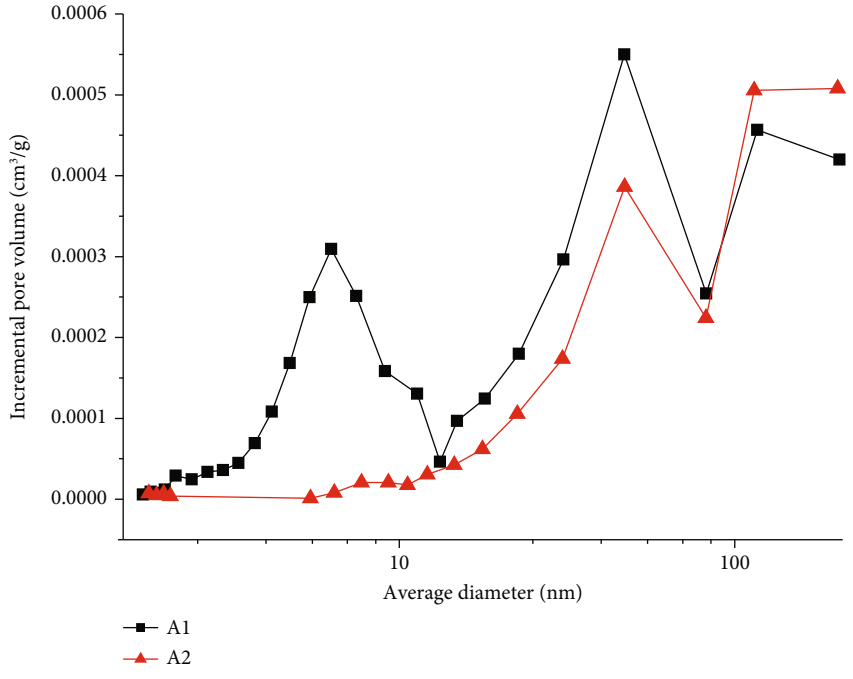

Figure 7: Comparison of liquid nitrogen pore volume of coal samples at different positions.

3.3.2. Pore Volume Comparison. After the action of small faults, the pore volume of micropores (<10 nm) and transition pores (10~100 nm) of coal samples has been greatly improved. In particular, a peak value is formed at 2~10 nm, indicating that the pore volume of micropores increases significantly (Figure 7). Compared with sample A2, the result shows that the total pore volume of sample A1 is increased by 1 time, and the pore volume of mesopore is increased by 4 times. The average pore diameter decreased by more than 2/3, which may be due to the rupture of some large pores into small holes under the action of faults.

3.3.3. Comparison of Specific Surface Area. After the action of small faults, the pore specific surface area of coal

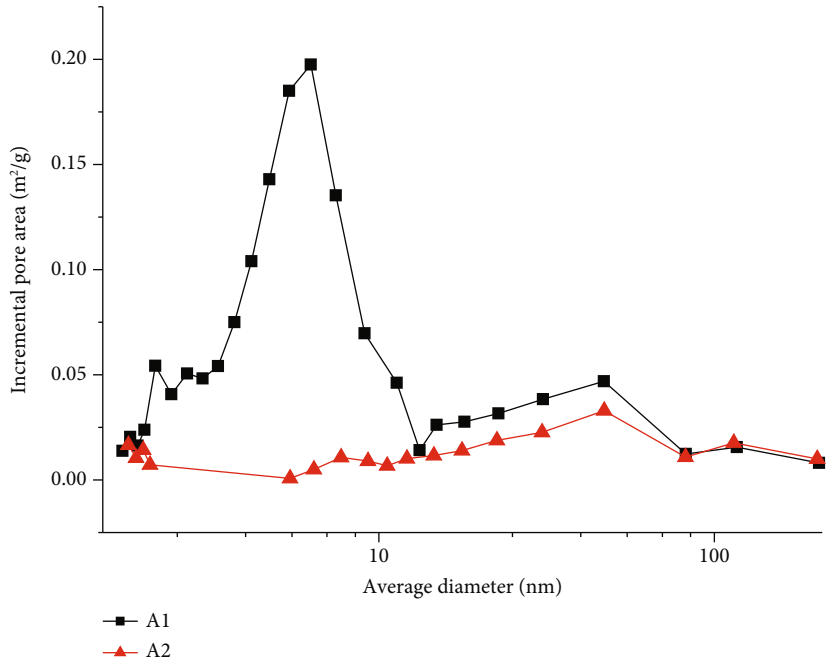

Figure 8: Comparison of liquid nitrogen specific surface area of coal samples at different positions.

samples has also been greatly improved. The specific surface area of coal sample A1 at the fault formed a peak in the pore size range of 2~10 nm, indicating that the number of micropores increased significantly. The results are consistent with mercury injection data (Figure 8). The test results show that compared with coal sample A2 without fault, the total specific surface area of coal sample A1 at fault increases by 6~7 times, in which the specific surface area of mesopore increases by 12 times and the specific surface area of micropore increases by 1 time (Table 3).

From the results of mercury intrusion and liquid nitrogen, it can be seen that the small faults have an obvious transformation effect on the pore structure of coal, causing the large pores inside the coal body to suffer a certain degree of damage, while the number of transition pores and micropores increases significantly, and the connectivity between pores is also enhanced.

Table 3: Comparison of liquid nitrogen test parameters of coal samples.

Sample	A1	A2
Total pore volume (cm^3/g)	4.1×10^{-3}	2.1×10^{-3}
Micropore volume (cm^3/g)	1.4×10^{-3}	6.0×10^{-5}
Transition hole pore volume (cm^3/g)	1.8×10^{-3}	1.1×10^{-3}
Medium and large pore volume (cm^3/g)	8.8×10^{-4}	1.0×10^{-3}
Total specific surface area (m^2/g)	1.5	2.3×10^{-1}
Micropore specific surface area (m^2/g)	1.2	6.5×10^{-2}
Transition pore specific surface area (m^2/g)	3.0×10^{-1}	1.2×10^{-1}
Medium and macropore specific surface area (m^2/g)	3.6×10^{-2}	3.9×10^{-2}
Average pore size (nm)	1.1×10^{1}	3.7×10^{1}

3.4. Raman Spectroscopy. The Raman characteristics of coal samples are closely related to the internal structure and molecular order of organic molecules [34–36]. The D peak, which is called the disordered peak, is due to the existence of lattice defects or heteroatoms in the coal macromolecules. The D peak area depends on the defects in the macromolecular structure of coal. The G peak is the unique graphene-like characteristic peak in the Raman spectrum. The G-band is related to the stretching vibration of C=C and represents the degree of order in the molecular structure. The area of the G peak is positively correlated with the total amount of aromatic rings and the enrichment degree of aromatic carbon in the macromolecular structure of coal [31, 37, 38].

The peak positions and curve trends of the Raman spectra of coal samples at different positions are basically the same. There are two obvious Raman vibration peaks, namely, D peak and G peak, in the wavenumber range of 1000-1800 cm^{-1} in the Raman spectrum. The peak position of D peak is 1350 cm^{-1}, and the peak position of G peak is 1600 cm^{-1} (Figure 9).

In order to quantitatively study the effect of faulting on the chemical composition and functional groups of coal, Gaussian fitting of Raman spectra was performed with OriginPro, and the Raman peak fitting diagram and

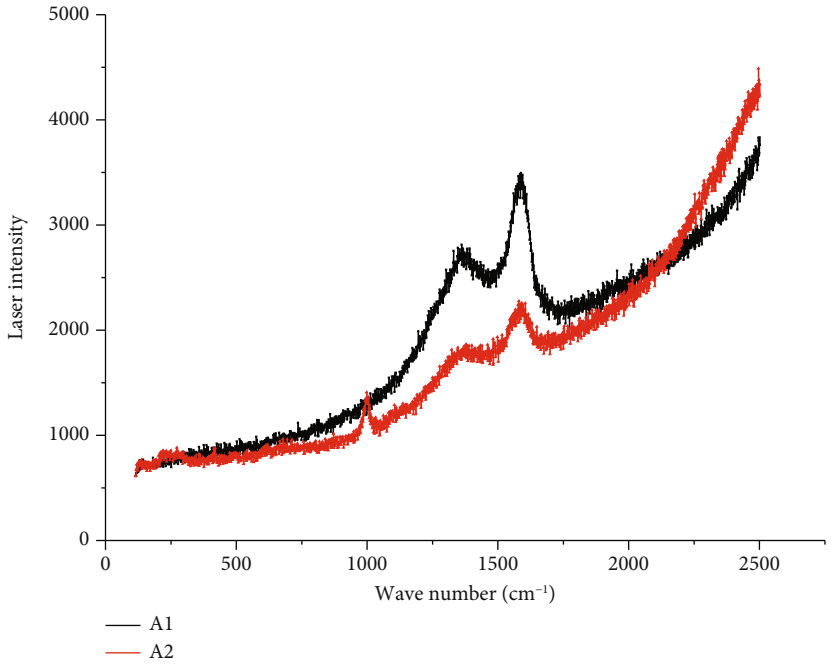

Figure 9: Comparison of Raman spectrum of coal samples at different positions.

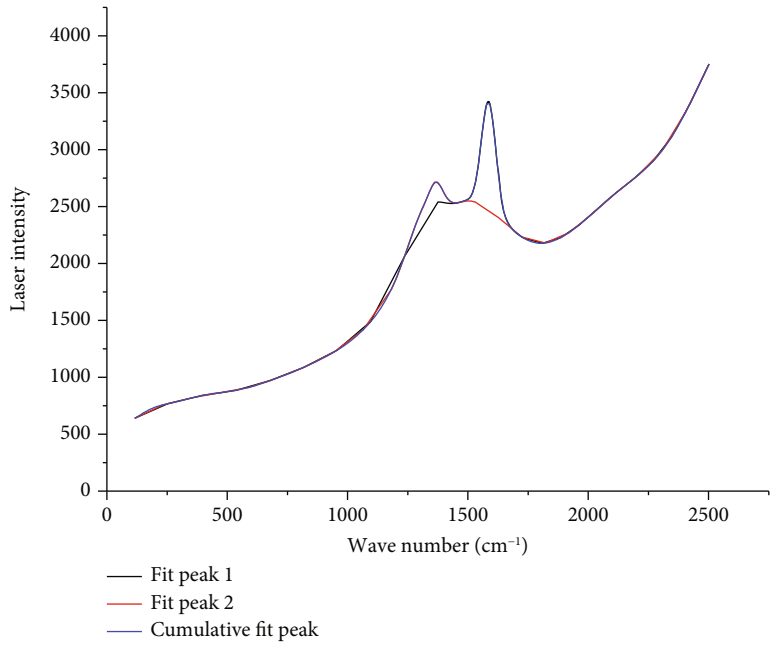

Figure 10: Fitting curve of Raman peaks of coal sample A1 at the fault.

Raman peak fitting parameters of coal samples at different positions were obtained (Figures 10 and 11, Table 4); the R^2 of all fitting results is greater than 0.95, indicating that the accuracy and reliability of the fitted data are high.

Based on the peak fitting results, five peak fitting parameters, including peak position, peak area, peak area percentage, peak intensity, and peak half-width of the characteristic peak, were selected to quantitatively analyze the effect of faulting on the macromolecular morphology of coal samples. Compared with the coal sample A2 without the fault, the D peak area of the coal sample A1 at the fault decreases, the peak intensity increases, and the half-peak width decreases. The result indicates that the amorphous carbon content decreases. The G peak area of coal sample A1 at the fault increased by about 1 time, the peak intensity increased by 1 to 2 times, and the half-peak width decreased, indicating

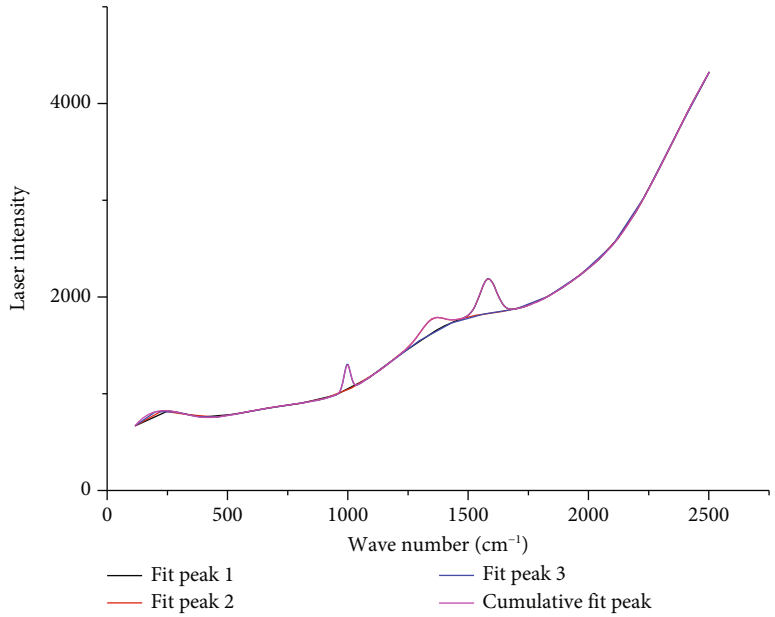

Figure 11: Fitting curve of Raman peaks of coal sample A2 without the fault.

Table 4: Comparison of Raman peak characteristics of coal samples.

Peak number	Peak area	Peak area percentage	Peak position	Peak intensity	Peak width at half maximum
A1-1	70566	85	1600	947	70
A2-1	30637	55	1600	356	81
A1-2	12363	15	1350	176	66
A2-2	16340	29	1350	141	109
A2-3	8989	16	1000	267	32

that the content of aromatic carbon increased. This result proves that faulting leads to the ordering process of coal.

4. Conclusions

(1) Small faults form directionally arranged fracture groups near the fault plane, which provides an enrichment place for gas storage. It is the key field of coal and gas outburst prevention and treatment

(2) Small faults affect the mesopores, shift the peak pore size from 1000 nm to 200~400 nm, and enhance the connectivity between pores. The number of transition pores and micropores is increased, especially the number of micropores which is greatly increased, and abundant ink bottle pores are formed

(3) The intensity of each peak position of Fourier infrared spectrum of coal sample at the fault increases, the area of D peak of the Raman spectrum decreases, and the area of G peak increases; that is, faulting also affects the structural composition of coal, which proves that faulting enhances the order of coal macromolecular structure

Data Availability

The data used to support the findings of this study are included within the article.

Conflicts of Interest

The authors declare that they have no conflicts of interest to report regarding the present study.

Acknowledgments

We would like to express appreciation for the following financial support: the National Natural Science Foundation of China, grant numbers 41972177, 41872169, and 42172189; the China Postdoctoral Science Foundation, grant number 2018M642747; Tackling Key Scientific and Technological Problems in Henan Province, grant number, 222102320346; and the National Natural Science Foundation of Henan Province, grant number 202300410099.

References

[1] Y. Li, S. Q. Pan, S. Z. Ning, L. Y. Shao, Z. H. Jing, and Z. S. Wang, "Coal measure metallogeny: metallogenic system and

implication for resource and environment," *Science China Earth Sciences*, vol. 65, no. 7, pp. 1211–1228, 2022.

[2] F. Chen, H. C. Yu, Z. F. Bian, and D. Y. Yin, "How to handle the crisis of coal industry in China under the vision of carbon neutrality," *Journal of China Coal Society*, vol. 46, no. 6, pp. 1808–1820, 2021.

[3] Y. Li, J. H. Yang, Z. J. Pan, S. Z. Meng, K. Wang, and X. L. Niu, "Unconventional natural gas accumulations in stacked deposits: a discussion of upper paleozoic coal-bearing strata in the east margin of the Ordos basin, China," *Acta Geologica Sinica*, vol. 93, no. 1, pp. 111–129, 2019.

[4] Y. Li, Z. S. Wang, S. H. Tang, and D. Elsworth, "Re-evaluating adsorbed and free methane content in coal and its ad- and desorption processes analysis," *Chemical Engineering Journal*, vol. 428, article 131946, 2022.

[5] J. B. Liu, Z. M. Song, B. Li, J. G. Ren, F. Chen, and M. Xiao, "Experimental study on the microstructure of coal with different particle sizes," *Energies*, vol. 15, no. 11, p. 4043, 2022.

[6] J. C. Cai, W. Wei, X. Y. Hu, R. C. Liu, and J. J. Wang, "Fractal characterization of dynamic fracture network extension in porous media," *Fractals*, vol. 25, no. 2, article 1750023, 2017.

[7] M. J. Li, S. Q. Lu, C. F. Wang, J. Liu, J. Shi, and T. B. Bei, "Effect of fragmentation on pore structures and fractal characteristics of intact coal and deformed coal based on experiments," *Geofluids*, vol. 2022, Article ID 8771617, 18 pages, 2022.

[8] Y. Bao, Y. W. Ju, Z. S. Yin, J. L. Xiong, G. C. Wang, and Y. Qi, "Influence of reservoir properties on the methane adsorption capacity and fractal features of coal and shale in the upper Permian coal measures of the South Sichuan coalfield, China," *Energy Exploration & Exploitation*, vol. 38, no. 1, pp. 57–78, 2020.

[9] A. Rabbani, M. Babaei, R. Shams, Y. Wang, and T. Chung, "DeePore: a deep learning workflow for rapid and comprehensive characterization of porous materials," *Advances Water Resources*, vol. 146, article 103787, 2020.

[10] D. A. Wood, "Techniques used to calculate shale fractal dimensions involve uncertainties and imprecisions that require more careful consideration," *Advances in Geo-Energy Research*, vol. 5, no. 2, pp. 153–165, 2021.

[11] Y. Li, C. Zhang, D. Z. Tang et al., "Coal pore size distributions controlled by the coalification process: an experimental study of coals from the Junggar, Ordos and Qinshui basins in China," *Fuel*, vol. 206, pp. 352–363, 2017.

[12] Y. Li, J. H. Yang, Z. J. Pan, and W. S. Tong, "Nanoscale pore structure and mechanical property analysis of coal: an insight combining AFM and SEM images," *Fuel*, vol. 260, article 116352, 2020.

[13] L. Shen, D. Jia, H. W. Yin et al., "Structural analogue modeling and PIV finite strain analysis: implications to tectonic fracture prediction," *Geological Journal of China Universities*, vol. 22, no. 1, pp. 171–182, 2016.

[14] Z. X. He and Y. Liu, "Evolution mechanism of mining fissures of overlying strata containing fault," *Safety in Coal Mines*, vol. 48, no. 8, pp. 201–204, 2017.

[15] J. T. Chen, W. F. Tan, K. Ma, and Z. Q. Wang, "Research on rock crack evolution mechanism in small fault under high stress of deep mining," *Mining Research and Development*, vol. 38, no. 8, pp. 21–25, 2018.

[16] X. F. Xu, "Numerical simulation of formation mechanism and distribution regularities of structural coal in thrust faults," *Coal Geology & Exploration*, vol. 40, no. 2, pp. 6–8, 2012.

[17] B. Zhou and K. L. Xu, "Study on influences of fault on coal and gas outburst in mining working face," *Coal Technology*, vol. 37, no. 9, pp. 218–221, 2018.

[18] B. Y. Jiang, Y. Zhao, B. Q. Lin, and T. Liu, "Effect of faults on the pore structure of coal and its resultant change on gas emission," *Journal of Petroleum Science and Engineering*, vol. 195, article 107919, 2020.

[19] R. Zhou, X. Z. Cheng, W. W. Su, and L. Zhu, "Study on pore structure and gas adsorption and desorption characteristics of coal in reverse fault area," *Safety in Coal Mines*, vol. 52, no. 9, pp. 22–28, 2021.

[20] X. S. Li, J. Wang, Z. Li, K. X. Zhang, X. Q. Feng, and Z. X. Wang, "Impact of brittle deformation on pore structure evolution in shale: samples collected from different fault positions," *Energy & Fuels*, vol. 36, no. 3, pp. 1441–1456, 2022.

[21] H. J. Zhu, Y. W. Ju, C. Huang et al., "Pore structure variations across structural deformation of Silurian Longmaxi Shale: an example from the Chuandong Thrust-Fold Belt," *Fuel*, vol. 241, pp. 914–932, 2019.

[22] X. L. Wang, Y. P. Cheng, D. M. Zhang, Z. D. Liu, Z. Y. Wang, and Z. G. Jiang, "Influence of tectonic evolution on pore structure and fractal characteristics of coal by low pressure gas adsorption," *Journal of Natural Gas Science and Engineering*, vol. 87, article 103788, 2021.

[23] M. Wang and Y. W. Wang, "SEM analysis of coal microstructure in Pingdianshan mining area," *Safety in Coal Mines*, vol. 45, no. 7, pp. 169–172, 2014.

[24] C. Y. Yang, H. Z. Chang, X. H. Shao et al., "Study on micropore characteristics of structural coal in different coal bodies under scanning electron microscopy," *Coal Science and Technology*, vol. 47, no. 12, pp. 194–200, 2019.

[25] B. Li, J. G. Ren, J. B. Liu, G. F. Liu, R. S. Lv, and Z. M. Song, "Diffusion and migration law of gaseous methane in coals of different metamorphic degrees," *International Journal of Heat and Technology*, vol. 37, no. 4, pp. 1019–1030, 2019.

[26] A. Golparvar, Y. Zhou, K. Wu, J. Ma, and Z. Yu, "A comprehensive review of pore scale modeling methodologies for multiphase flow in porous media," *Advances in Geo-Energy Research*, vol. 2, no. 4, pp. 418–440, 2018.

[27] J. G. Zhang, X. Y. Li, J. H. Jiao, J. B. Liu, F. Chen, and Z. M. Song, "Comparative study of pore structure characteristics between mudstone and coal under different particle size conditions," *Energies*, vol. 14, no. 24, p. 8435, 2021.

[28] J. G. Ren, Z. M. Song, B. Li, J. B. Liu, R. S. Lv, and G. F. Liu, "Structure feature and evolution mechanism of pores in different metamorphism and deformation coals," *Fuel*, vol. 283, article 119292, 2021.

[29] L. Zhang, N. I. Aziz, T. Ren, J. Nemcik, and S. Tu, "Influence of coal particle size on coal adsorption and desorption characteristics," *Archives of Mining Sciences*, vol. 59, no. 3, pp. 807–820, 2014.

[30] K. Z. Zhang, *Fine Quantitative Characterization of Tectonic Coal Microstructure and Research on Gas Fractal Transport Characteristics*, China University of Mining and Technology, Xuzhou, 2020.

[31] A. P. Nikitin, Y. N. Dudnikova, E. S. Mikhaylova, and Z. R. Ismagilov, "Raman characteristics of Kuznetsk basin coal and coal-based sorbents," *Coke and Chemistry*, vol. 62, no. 9, pp. 379–384, 2019.

[32] F. Košek, H. G. M. Edwards, and J. Jehlička, "Raman spectroscopic vibrational analysis of the complex iron sulfates clairite,

metavoltine, and voltaite from the burning coal dump Anna I, Alsdorf, Germany," *Journal of Raman Spectroscopy*, vol. 51, no. 9, pp. 1454–1461, 2020.

[33] M. J. Blunt, B. Bijeljic, H. Dong et al., "Pore-scale imaging and modelling," *Water Resources*, vol. 51, pp. 197–216, 2013.

[34] B. Li, F. Chen, P. W. Jiang, J. G. Ren, J. B. Liu, and Z. M. Song, "Study on structure evolution features of different rank coals under shock load," *Coal Science and Technology*, vol. 49, no. 10, pp. 217–227, 2021.

[35] B. Li, J. B. Liu, J. G. Ren, F. Chen, and Z. M. Song, "Experimental study of influence of hydraulic punching on microscopic pores and structural components of coal," *Coal Science and Technology*, vol. 49, no. 8, pp. 131–138, 2021.

[36] J. S. Lupoi, L. P. Fritz, P. C. Hackley, L. Solotky, A. Weislogel, and S. Schlaegle, "Quantitative evaluation of vitrinite reflectance and atomic O/C in coal using Raman spectroscopy and multivariate analysis," *Fuel*, vol. 230, pp. 1–8, 2018.

[37] Q. L. Hou and X. S. Li, "The effect of tectonic deformation on gas outburst and excess coal bed methane," *Physics*, vol. 43, no. 6, pp. 373–380, 2014.

[38] S. Potgieter-Vermaak, N. Maledi, N. Wagner, J. H. Van Heerden, R. Van Grieken, and J. H. Potgieter, "Raman spectroscopy for the analysis of coal: a review," *Journal of Raman Spectroscopy*, vol. 42, no. 2, pp. 123–129, 2011.